Macromolecular Research, Vol. 16, No. 5, pp 457-466 (2008)

Transport Properties of Polymer Blend Membranes of Sulfonated and Nonsulfonated Polysulfones for Direct Methanol Fuel Cell Application

Dong Hwee Kim and Sung Chul Kim*

Polymer Engineering Laboratory, Department of Chemical and Biomolecular Engineering (BK-21 Program), Korea Advanced Institute of Science and Technology, Daejeon 305-701, Korea

Received December 22, 2007; Revised February 8, 2008; Accepted February 9, 2008

Abstract: The relation between the phase separated morphologies and their transport properties in the polymer blend membrane for direct methanol fuel cell application was studied. In order to enhance the proton conductivity and reduce the methanol crossover, sulfonated poly(arylene ether sulfone) copolymer, with a sulfonation of 60 mol% (sPAES-60), was blended with nonsulfonated poly(ether sulfone) copolymer (RH-2000, Solvay). Various morphologies were obtained by varying the drying condition and the concentration of the casting solution (10, 15, 20 wt%). The transport properties of proton and methanol molecule through the polymer blend membranes were studied according to the absorbed water. AC impedance spectroscopy was used to measure the proton conductivity and a liquid permeability measuring instrument was designed to measure the methanol permeability. The state of water in the blend membranes was confirmed by differential scanning calorimetry and was used to correlate the morphology of the membrane with the membrane transport properties.

Keywords: direct methanol fuel cell (DMFC), blend membrane, phase separation, proton conductivity, methanol crossover, selectivity.

Introduction

Stimulated by legislative pollution control and with most industrialized nations facing a rapid depletion of traditional energy sources, fuel cells have been targeted as next-generation alternative power sources. A fuel cell is an energy conversion system that converts chemical energy directly into electrical energy with higher efficiency and lower emission of pollutants than commercial internal combustion engines.[1] The Direct Methanol Fuel Cell (DMFC) is considered to hold the strongest potential for application in small sized devices such as portable electric appliances. The DMFC system is easily initiated because of its low operating temperature. Furthermore, its simple structure facilitates easy fabrication: a fuel vaporizer, complex humidification, and thermal management systems are not required. Fuel storage and supply are also safe, because methanol is chemically stable and is used in a liquid state in the operating condition.[2] The high energy density of methanol also facilitates application to portable devices, because the integration of various functions into one unit requires concentrated power density.

Despite offering many strengths, the DMFC also has some notable limitations, including poor adhesion between the membrane and electrodes, low activity of the electrodes, and crossover of unreacted fuel through the membrane.[3] Methanol crossover induces an unexpected drop in the open circuit voltage and therefore the overall efficiency of the system decreases.[4] Various solutions to these problems have been proposed, such as synthesis of cost-effective alternative polymers [5-10] and blending of organic-inorganic compounds or acid-doped polymers.[11-15] However, they fail to adequately mitigate loss in the proton conductivity when the methanol permeability is reduced.

In the present study, a polymer-polymer blend membrane composed of a proton conductive component and a methanol barrier component was prepared. In order to obtain excellent proton conductivity of the blend membrane highly sulfonated poly(arylene ether sulfone)copolymer with 60 mole percent of disulfonated comonomer (sPAES-60) was synthesized via a poly-condensation reaction. A poly(ether) sulfone copolymer (RH-2000), obtained from Solvay, may contribute to an enhancement of the chemical and mechanical stability and a reduction of methanol crossover. Various morphologies were induced by controlling the drying condition and the concentration of the casting solution without changing blend ratio. On the basis of the morphological features, phase separated blend membranes were categorized

*Corresponding Author. E-mail: kimsc@kaist.ac.kr

into four groups: layered structure (Group I), large isolated domains (Group II), nodular structure (Group III), and fully co-continuous morphology (Group IV).[11]

In this paper, the proton and methanol transport phenomena through the membrane were investigated. The proton transport mechanism in the polymer electrolyte is very complex and has been widely studied. Although there is strong consensus on the feasibility of both vehicle and hopping mechanisms, distinguishing between these two mechanisms is difficult as the two models are thought to be in operation simultaneously in most cases.[16-19] The proton conductivity is dependent on the hydrated state of the membrane, because the protons are solvated and can thus be transported through the membrane in a water swollen membrane. Ultimately, the correlation between the morphology of the membrane and membrane transport properties was verified on the basis of the state of water.

Experimental

As reported in previously published paper,[11] sPAES-60 was synthesized from disulfonated 4,4′-dichlorodiphenylsulfone (SDCDPS, 3.3 mmol), 4,4′-dichlorodiphenylsulfone (DCDPS, 2.2 mmol), and 4,4′-biphenol (BP, 5.5 mmol) based on anhydrous NMP medium. After dehydrating the reaction mixture under reflux at 160 °C for 4 h, the reaction compound was gradually heated to 190 °C for 18 h to complete dehydration of the reacting compound. RH-2000 synthesized from 4,4′-dihydroxydiphenyl-sulfone (bisphenol S) and 4,4′-dichlorodiphenylsulfone was obtained from Solvay. Two component polymers were dissolved in dimethylacetamide (DMAc) with 10, 15, and 20 wt% and blended with 1 to 1 weight based blend ratio. In order to vary the rate of phase separation the blend membranes were prepared via different procedures: HT (drying at 80 °C under ambient atmosphere for 12 h followed by further drying at 120 °C under vacuum for 24 h), FD1 (freeze drying at -20 °C under vacuum for 80 h followed by drying at 100 °C for 24 h), and FD2 (freeze drying at -75 °C under vacuum for 140 h followed by drying at 100 °C for 24 h). More detailed membrane fabrication process is described in another paper.[11] Figure 1 shows the result of the phase separation in the blend membranes observed by scanning electron microscopy. All the prepared membranes were acidified by immersion in a 0.5 M sulfuric acid aqueous solution at 25 °C for 24 h and then rinsed while being immersed in deionized water for 24 h. The deionized water was replaced by fresh deionized water every 4 h during the immersion.

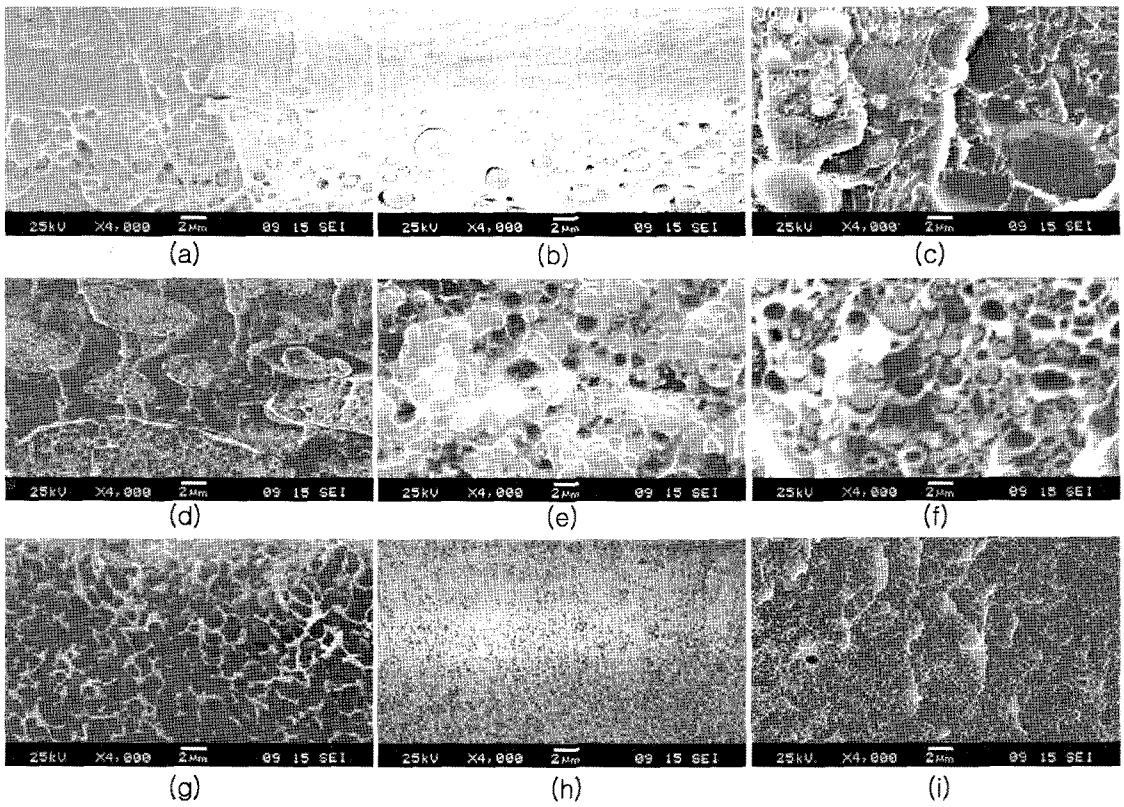

Figure 1. SEM micrographs: freeze fractured cross-section, sPAES-60: RH-2000=1:1 (a) sample 1 (HT 10 wt%), (b) sample 2 (HT 15 wt%), (c) sample 3 (HT 20 wt%), (d) sample 4 (FD1 10 wt%), (e) sample 5 (FD1 15 wt%), (f) sample 6 (FD1 20 wt%), (g) sample 7 (FD2 10 wt%), (h) sample 8 (FD2 15 wt%), (i) sample 9 (FD2 20 wt%). Images were reprinted from reference [11].

Characterization

Water Uptake. Acidified membranes were equilibrated in deionized water at room temperature for 24 h to remove extra sulfuric acid and then vacuum-dried at 100 °C for 24 h, weighed, and immersed in deionized water at 25 °C for 24 h. Surface water was wiped away and the membranes were quickly weighed again to obtain the exact water absorption. Weight based water uptake (WU_W) was calculated by the ratio of weight gain to the original membrane according to eq. (1). To estimate the dimensional stability, volume based water uptake was also considered. In this measurement, the volume of the wet membrane was very difficult to measure because the shape of the water absorbed membrane was not constant. Hence, the volume based water uptake was derived from the weight based water gain using the densities of the dry membrane and deionized water according to eq. (2)

$$WUw(\%) = \frac{w_{wet} - w_{dry}}{w_{dry}} \times 100 \quad (1)$$

$$WUv(\%) = \frac{(w_{wet} - w_{dry})/\rho_w}{w_{dry}/\rho_m} \times 100 \quad (2)$$

where w_{wet} and w_{dry} are the weights of wet and dried membranes, and ρ_w and ρ_m are the densities of water (1 g/cm^3) and the dry membrane (1.41 g/cm^3).

States of Water. The state of water in the membrane was analyzed using DSC (TA instrument Q100). To ensure the effective sealing, the aluminum sample pan was replaced with a high pressure capsule. After the surface water was removed, the fully hydrated membrane specimen was rapidly placed in the capsule to eliminate water loss during sample preparation. The sample and sealed capsule assembly were cooled and held at -50 °C for 60 min to bring the capsule kit to equilibrium and then heated to 50 °C at a heating rate of 1 °C/min. The amount of free water was quantified from the ratio of the integrated area of the melt endothermic peak at 0 °C to the heat of fusion (334 J/g) of pure water. The integration of the melting endothermic peak was performed by a Universal analysis 2000. Bound water was estimated by subtracting the free water content from the total water uptake in the blend membranes.

Proton Conductivity. The proton conductivity in the through-plane direction of the membranes was measured by the AC impedance spectroscopy technique over a frequency range 0.1-10 MHz with AC perturbation of 10 mV, using a Solatron 1255 impedance/gain-phase analyzer. The conductivity cell was immersed in a thermostat to maintain constant temperature. When the proton conductivity was measured at a different temperature, the cell including the membrane was equilibrated in the thermostat for 5 h so as to be adapted to the adjusted temperature. The proton conductivity was calculated from the following correlation (eq. (3)).

$$\sigma = \frac{d}{RS} \quad (3)$$

where σ is the proton conductivity (S/cm), membrane thickness d is the same as distance between the electrodes used to measure the potential, surface area S (S=1.03 cm^2) is the sames as the surface area of the electrodes, and R is the impedance, which is determined from a linear regression to x-intercept over a high frequency ranges when the imaginary impedance is equal to zero. The measurement was performed 10 times for each sample and in every case impedance was collected after the Nyquist diagram was stable at a constant value.

Methanol Permeability. The methanol permeability was obtained by calculating the methanol flux through the membrane. The membrane was placed into a glass cell comprised of double baths. They were then immersed in the thermostat to maintain constant temperature. One bath was filled with methanol solution (5 wt% in deionized water), and the other with pure deionized water to reproduce a phenomenon of methanol crossover in DMFC system. The solution in each bath was stirred with a magnetic stirrer during measurement. Initially, the correlation between methanol concentration and refractive index was assessed using an Abbe refractometer (ATAGO 3T). The sample was removed from the bath using a microsyringe to measure the refractive index, which in turn informed the methanol concentration. Sampling was performed every 10 min for a total duration of 300 min for each sample. Because of the difference in methanol concentration between neighboring baths, a concentration gradient was formed through the membrane. The methanol concentration can be expressed as eq. (4) as a function of time

$$C_B(t) = S \cdot D \cdot K \cdot C_{A0} \frac{(t - t_0)}{V_B \cdot L} \quad (4)$$

where C_{A0} is the initial concentration of methanol, L membrane thickness, S surface area, and V_B the volume of deionized water bath. Methanol diffusivity and sorption coefficient of the membrane are denoted as D and K, respectively. The methanol permeability can be obtained from the product of D and K, which is estimated from the regressed slope of $C_B(t)$ vs. time.

Results and Discussion

Morphology and Water Absorption. The morphologies of the blend membranes observed by SEM were classified into four groups: two-layer structure (Group I), isolated domains (Group II), nodular structure (Group III), and co-continuous morphology (Group IV) (Figure 1). They showed different amount of water absorption in spite of the same composition between component polymers (Table I). Although three kinds of Groups (I, III, and IV) showed sim-

Table I. Summary of Morphology, Water Uptake, and States of Water for Hydrated Membranes

Samples	Condition	Morphology	λ^a			Water Uptake (%)	
			Total	Bound	Free	Weight	Volume
Sample 1	10 wt% HT	Layered structure	18.2	15.1	3.1	68.3	96.4
Sample 2	15 wt% HT	Layered structure	18.0	14.6	3.4	67.7	95.5
Sample 3	20 wt% HT	Isolated big domains	15.1	10.9	4.2	56.9	80.2
Sample 4	10 wt% FD1	Isolated big domains	15.2	10.3	4.9	57.3	80.8
Sample 5	15 wt% FD1	Nodular structure	19.0	12.9	6.1	71.8	101.3
Sample 6	20 wt% FD1	Nodular structure	18.7	12.5	6.2	70.7	99.7
Sample 7	10 wt% FD2	Nodular structure	18.4	12.0	6.4	70.1	98.9
Sample 8	15 wt% FD2	Co-continuous	19.5	12.3	7.2	75.3	106.2
Sample 9	20 wt% FD2	Co-continuous	20.0	12.3	7.7	75.8	106.9
Nafion117	-	-	19.5	10.5	9.0	20.1	40.0
sPAES-60	-	-	48.0	35.4	12.6	152.5	231.8
RH-2000	-	-	0	0	0	1.1	1.4

λ^a: The number of water molecules per sulfonic acid group.

ilar values in water uptake, Group II absorbed the smallest amount of water among the blend membranes, and thus showed the lowest values in weight and volume based water uptakes and total number of water molecules per sulfonic acid group. As confirmed in a previous article,[11] this is attributed to the isolated domains of sPAES-60 which played significant role in the water absorption. sPAES-60 is a very hydrophilic polymer and its water uptake is 152.5% in weight but these are encapsulated by hydrophobic RH-2000 domains and thus hydrophilic domains are partially un-accessible in Group II.

On the basis of a comparison of Group II and Group III, it was assumed that the continuity of hydrophilic domains is more important to increase water uptake of membranes than the sizes of the hydrophilic domains. Group II had a higher value of average domain size (7.9 μm for HT 20 wt%, 8.2 μm for FD1 10 wt%) than Group III (2.2 μm for FD1 15 wt%, 2.0 μm for FD1 20 wt%, and 1.5 μm for FD2 10 wt%). Although the relatively large sPAES-60 domains in Group II could contribute to greater water uptake than other smaller domains, AFM analysis indicated that the hydrophilic region of Group II was captured in the hydrophobic matrix.[11] As a result, Group III, with partially linked nodule-like sPAES-60 domains, showed higher water uptake.

In the case of Group IV, although SEM and EDAX results already informed the co-continuity of sample 8 (FD2 15 wt%) and sample 9 (FD2 20 wt%),[11] water uptake also could be an evidence of this morphology. Total water absorption of sPAES-60 and RH-2000 was 152.5 wt% and 1.1 wt%, respectively. In addition, two samples in Group IV showed 75.3 wt% and 75.8 wt% water uptake. Because these values were approximately the average of the total water absorption of the two components which were blended with 1 to 1 weight based blend ratio, the existence of a co-continuous structure in Group IV could be confirmed.

Volume based water uptake can be a tool to estimate the dimensional stability of a fuel cell during actual operation. sPAES-60 with extremely high volume expansion ratio (above 230 vol%) is not suitable for the preparation of the membrane electrode assembly (MEA) or stacking of unit cells. All the blend membranes used in this study enhanced dimensional stability, as volume based water uptake was reduced approximately to half that of sPAES-60.

State of Water. The examination of water states is a critical factor to elucidate the transport properties of DMFC membranes, as this is a more useful tool to correlate the trend of proton conductivity and methanol permeability with the distribution of water molecules than other variables. State of water in the sulfonated membranes is usually determined from the specific interaction between water and sulfonic acid group in the ionic domains. As reported in a current study,[20] the states of water within a polymer membrane can be distinguished as free water, weakly bound water, and strongly bound water. Free water is defined as water that is not closely associated with the polymer matrix and has the same phase-transition behavior as bulk water, i.e., a characteristic meting peak at 0 °C. Weakly bound water or 'freezable loosely bound water' is defined as water that is weakly connected to the polymer matrix or that interacts weakly with strongly bound water and displays a relatively broad melting endothermic peak at sub-zero temperature. Because this kind of water molecule is susceptible to the thermal experimental conditions, exact extraction is difficult. The last type is strongly bound water, sometimes

referred to as 'nonfreezing bound water', and is defined as water that is firmly bound to the polymer matrix. Because this type of water is enclosed in the polymer chains, it does not show a detectable thermal transition at sub-zero temperature but acts as a plasticizer by reducing the glass transition temperature of the polymer:

It is difficult to carry out the precise quantification of three states of water in the sulfonated polymer electrolyte membrane by DSC measurement alone because all the water molecules exist in an interchangeable continuous state and thus overlapping endothermic peaks are easily detected. However DSC technique proved a powerful means of determining the amount of free water by considering freezable water as free water and non-freezable water as bound water. Moreover, in this experiment, the characteristic melting peak at 0 °C was observed and no peaks were detected except around 0 °C in the samples (Figure 2) and therefore free water and bound water could be classified. After the amount of free water and bound water was calculated from a comparison with the heat of fusion of pure water (334 J/g), each content of water molecules was converted to the number of water molecules per sulfonic acid group ($\lambda_{[H_2O]/[-SO_3H]}$). The amount of each state of water is summarized in Table I. Contrary to the amount of total water uptake and the number of total water molecules based on the number of sulfonic acid groups, the number of free water molecules increased monotonously from sample 1 to sample 9 as the degree of continuity of the hydrophilic phase was increased. Thus, it was also determined that the number of free water molecules cannot be predicted precisely from only the total water uptake and number of total water molecules.

Proton Conductivity. The proton conductivity of the membrane in a proton exchange membrane fuel cell is a critical parameter with respect to the evaluation of a fuel cell system. Specifically, a higher value of proton conductivity allows higher power densities to be achieved. Proton conduction through the membrane is known to occur via two routes.[21] One is the Grotthus mechanism, sometimes called a hopping or jumping mechanism, in which a proton passes through pores or along a chain of water molecules.

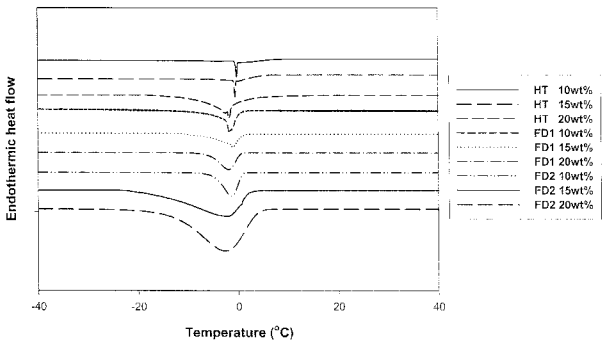

Figure 2. DSC heating thermograms.

These act as stationary vehicles, having only local motion. Hydrogen bonds are required to fulfill this type of conduction, and continuous motion is possible due to rapid reorientation of the solvent, thus providing a proton pathway. The other is the vehicle mechanism, in which a proton combines with a protonated vehicle (ex. H_3O^+, $CH_3OH_2^+$) or unprotonated vehicle (ex. H_2O), thereby allowing the net transport of protons. In this case, the proton moves at the rate of vehicular diffusion and the net proton transport is governed by vehicle diffusion rates due to the vehicle's counter diffusion. Proton conduction in blend membranes may occur by a mixed mechanism.

As noted above, nine samples were classified into four groups according to their morphological similarity. Figure 3 shows the proton conductivity of each group compared with that of Nafion117. In all cases, regardless of the drying condition and casting solution concentration, as temperature increased the proton conductivity also increased in the following order: Group I < Group II <Group III < Group IV. The proton conductivity of the membranes is closely related to the mobility of the water molecules in the membranes, which is influenced by electrostatic interaction with ionic species. If the interaction is stronger, the mobility of the water molecules in the membranes will be reduced and diffusion of the water molecules becomes difficult.[25,26]

It has known that the vehicle mechanism was predominant where PEMs have high water content while Grotthus mechanism was predominant where PEMs have low water content.[10] PEMs that have high water content have much higher conductivity because the vehicle mechasim is more effective. Proton conduction in the blend membrane may occur by a mixed mechanism: a partial vehicle type mechanism and a partial Grotthus type mechanism in the domain of sulfonic acid group and water complex. According to Table I, the trend of the number of free water molecules per sulfonic acid group (λ_{free}) showed a similar pattern to the proton conductivity. This serves as a clue to determining the proton transport mechanism. As reported in a previously published paper,[20] free water acts as a proton-carrying medium according to the vehicle mechanism, as it is not bound to the polymer matrix. Abundant of bound water is considered to help the Grotthus mechanism by using the hydrogen bonds between captured water molecules. As temperature increases the number of bound water molecules would decrease because of a breakdown of hydrogen bonds, and consequently the proton conduction occurring through the Grotthus mechanism would decrease at high temperature. However, as plotted in Figure 3, proton conductivity of the blend membrane was maintained even at higher temperature. This is because the decrease in proton conduction via the Grotthus mechanism was compensated by an increase in proton conduction via the vehicle mechanism by elevated proton mobility at high temperature. Group IV showed the highest proton conductivity. This is attributed to Group IV

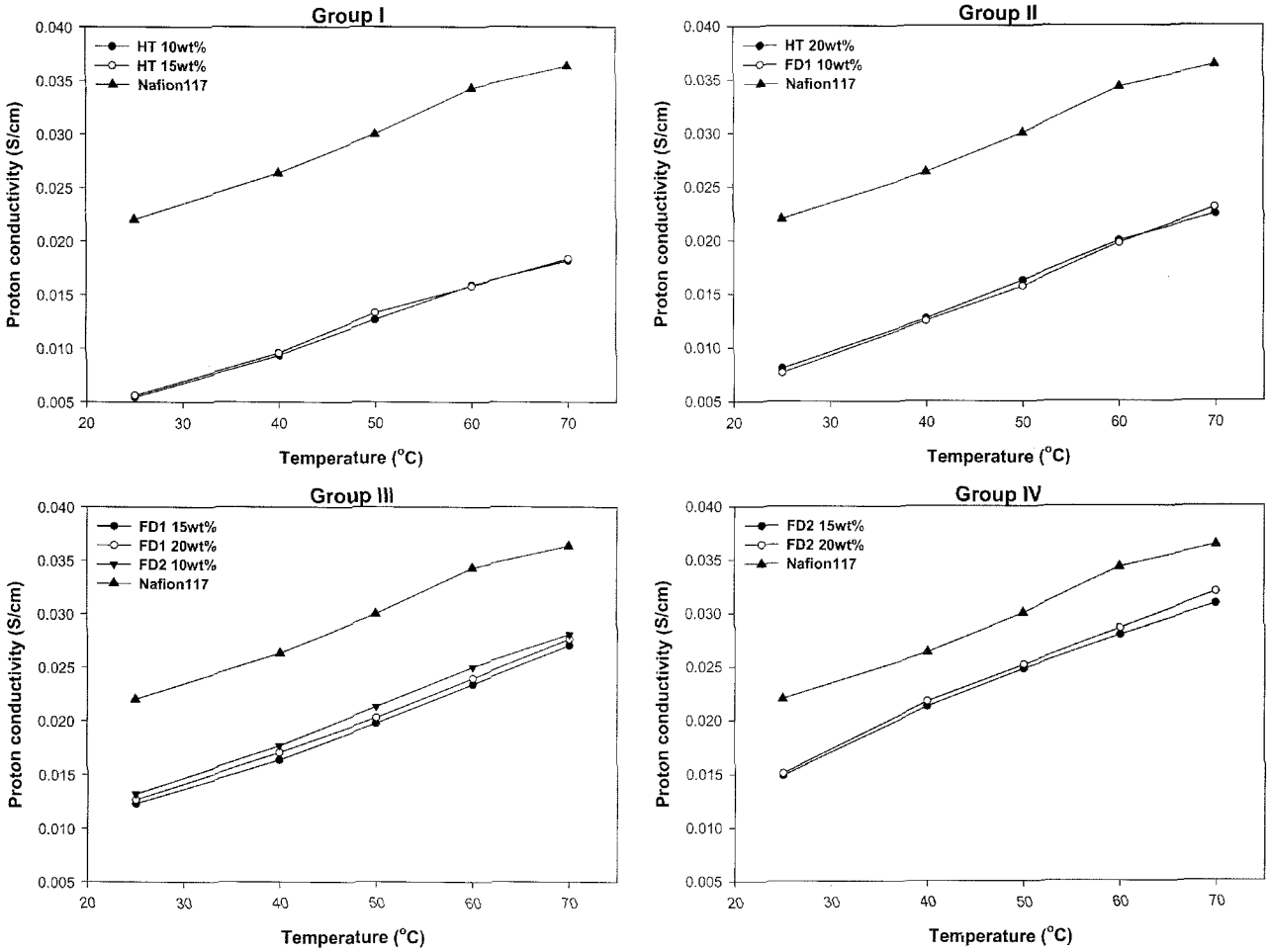

Figure 3. Proton conductivity of blend membranes.

having the largest number of free water molecules per unit sulfonic group (Figure 5), as well developed hydrophilic channels are ascribed to a fully hydrated percolated network of ions and free water.

Methanol Permeability. Methanol permeability is also one of the most important membrane properties in DMFC applications since methanol crossover from the anode to the cathode leads to lower cell voltage and fuel efficiency due to the loss of the unreacted fuel. Generally, transport properties are affected by the fraction of free water.[22] For example, as summarized in Table I, Nafion117 has the largest number of free water molecules in spite of having the lowest water uptake, and thus it could transport both protons and fuel simultaneously. Transport of water and methanol in the membrane depends on complex interactions between permeates and the polymeric membrane matrix.[23,24] In sPAES membranes, it can be assumed that certain distinct environments for mass transport of water and methanol exist such as a hydrophilic environment formed by highly polar sulfonic acid groups ($-SO_3H$), a hydrophobic environment of the polymeric matrix, which is the less polar part of the polymer, and the water and methanol bulk environment in the channels. Water preferentially interacts with the sulfonate groups of the polymer and methanol rather than with the polymer matrix, due to the chemical affinity. Methanol permeability of these groups is plotted in Figure 4. The trend of each group is similar to the proton conductivity trend. Overall values increase in the order of Group I < Group II <Group III < Group IV, but in all cases the amount of methanol permeability was less than the half of Nafion117 in the DMFC operating temperature. The rate of increase of methanol permeability is also different for each group. Group I showed a rapid increase above 50 °C, a similar tendency to that observed for the Nafion117. Generally, as temperature increases, the molecular diffusion is accelerated and the hydrophilic channels tend to be enlarged. Because layered structured samples maintained the property of the component polymer, the influence of sPAES-60 was revealed at high temperature. Methanol permeability increased monotonously in Group II but it was retarded above 50 °C in Group III and Group IV. The degree of retardation of Group IV was larger than that of Group III. This phenome-

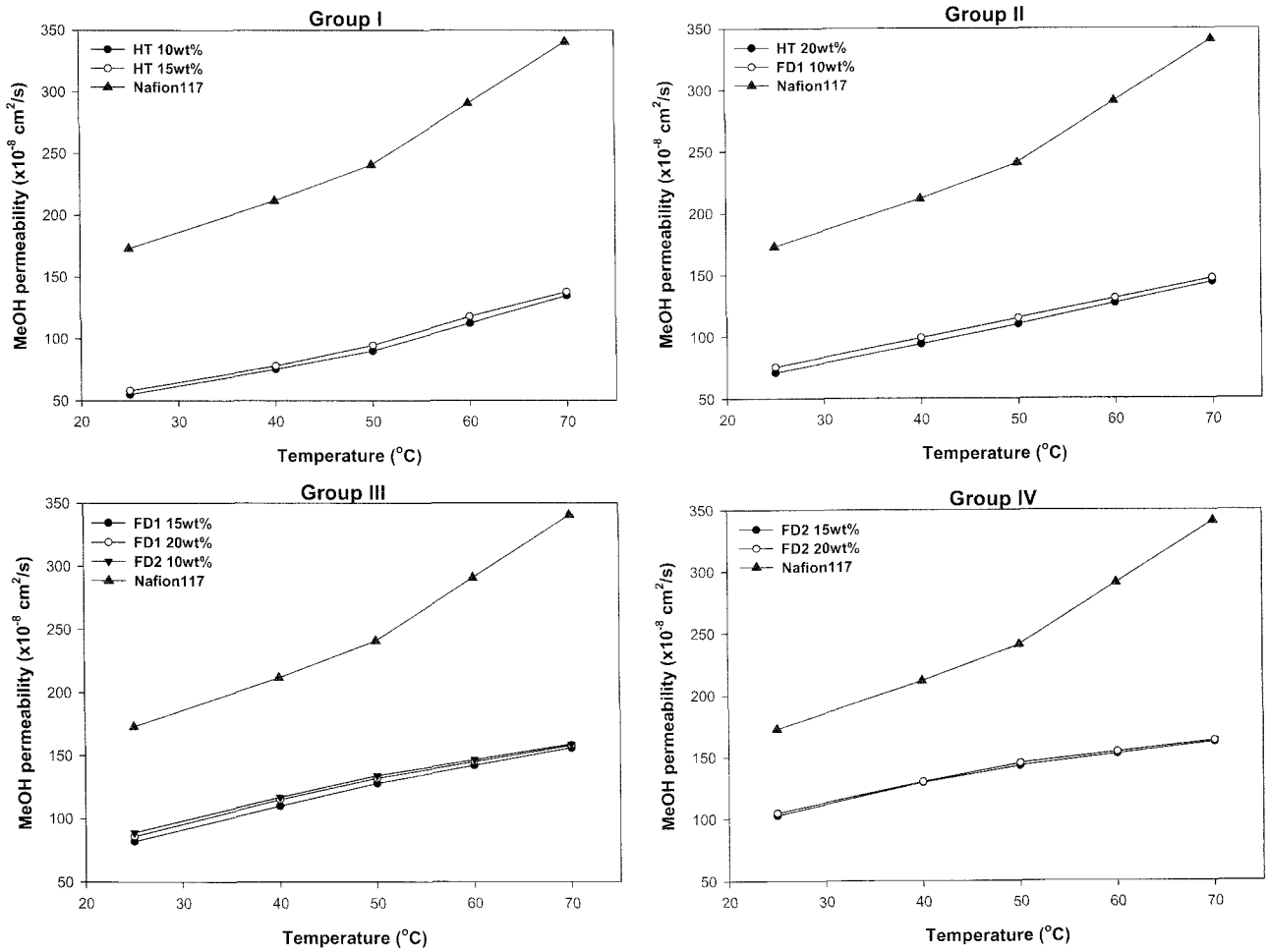

Figure 4. Methanol permeability of blend membranes.

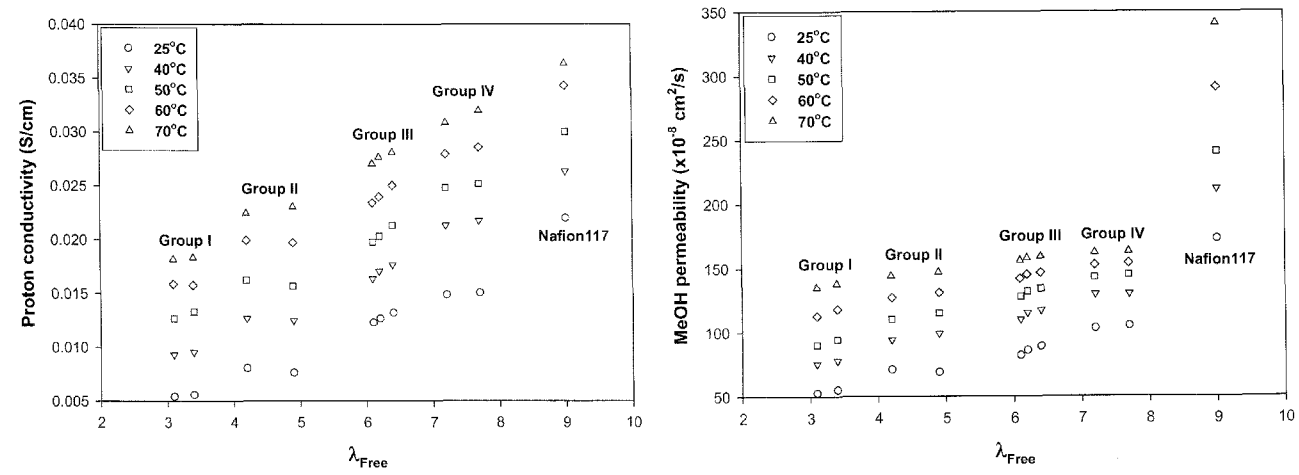

Figure 5. Plots of number of free water molecules and transport properties.

non is ascribed to the well-grown and co-continuous hydrophobic region in Group IV. Continuous hydrophobic channels would block methanol passage through the membrane and also restrict the enlargement of the hydrophilic channels as the temperature is increased. As shown in Figure 5, when proton conductivity and methanol permeability are plotted with the number of free water molecules, each group can be clearly delineated. Therefore, estimation of the number of free water molecules is very useful to predict the transport properties of a membrane without performing complex calculations.

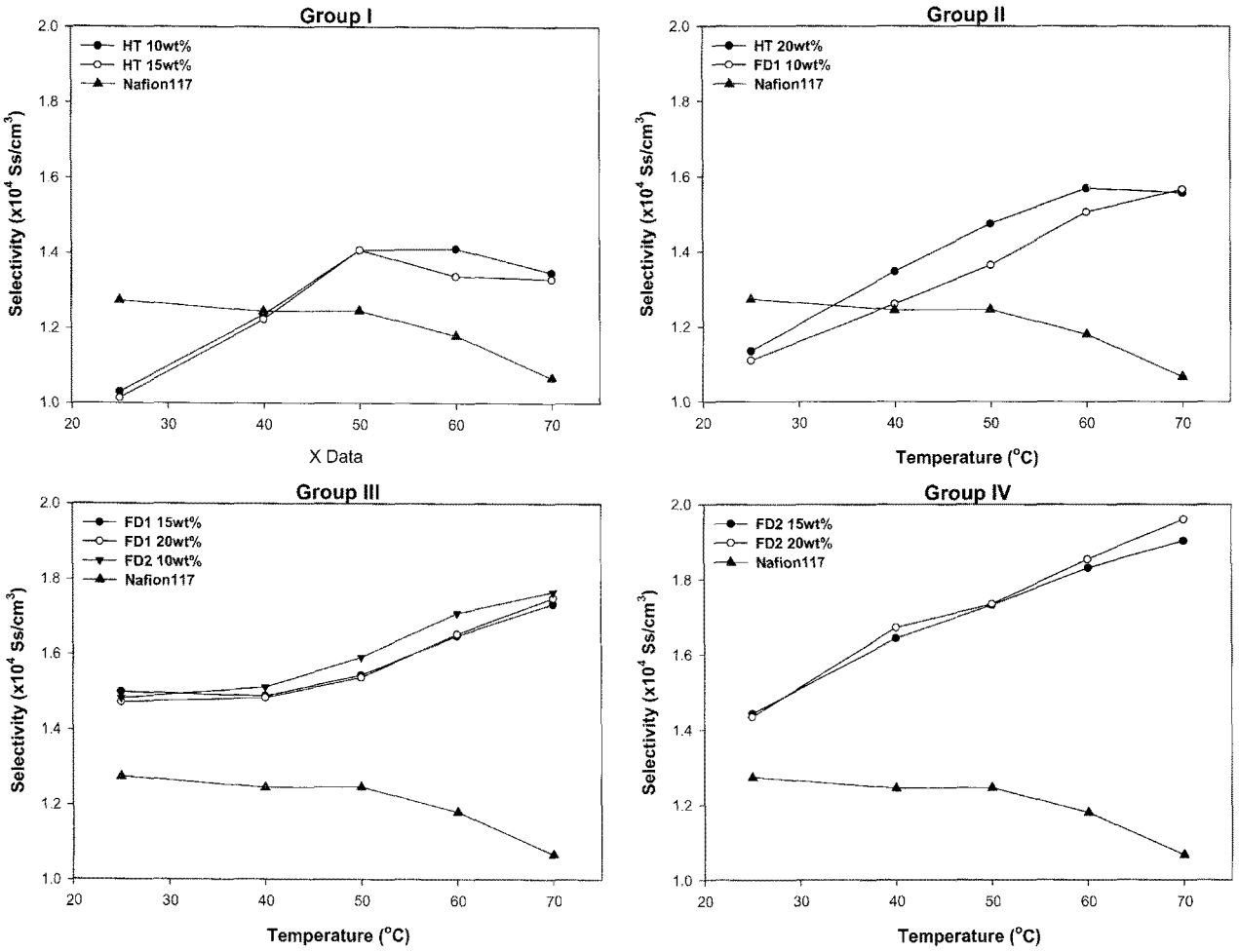

Figure 6. Membrane selectivity.

Selectivity. In order to apply the blend membrane to the DMFC system not only individual properties such as proton conductivity and methanol permeability but also membrane selectivity between the proton and methanol should be considered because membranes with high selectivity have the potential to show improved performance in DMFCs. Generally, selectivity of a DMFC membrane can be defined as given by eq. (5).

$$\text{Membrane selectivity} = \frac{\text{Proton conductivity}}{\text{Methanol permeability}} \tag{5}$$

Selectivity change of blend membranes according to the temperature can also be classified into four groups based on distinctive morphological characteristics of the membrane, as summarized in Figure 6. All nine samples showed higher selectivity than Nafion117 above 50 °C but each group showed a characteristic selectivity pattern. Selectivity of Nafion117 decreased as the temperature was increased, because methanol flooded through the membrane at high temperature whereas the blend system maintained high selectivity at this temperature. In spite of the lowest methanol permeability of Group I below 50 °C, the selectivity of Group I and Group II was lower than Nafion117 because hydrophobic layer also repressed proton conduction. In the case of Group II, selectivity increased monotonously with temperature, and above 40 °C it was higher than that of Nafion117. Group III and Group IV showed a similar pattern to Group II but selectivity at low temperature was better than that of Group II. The highest selectivity in high temperature was observed in Group IV. The most significant difference in selectivity between Nafion117 and the blend membranes was observed above 40 °C. As discussed in the previous section, at this temperature the methanol permeability of Nafion117 rapidly increased whereas the blend system effectively inhibited fuel crossover.

As summarized in Figure 7, relative transport properties could serve as reliable evidence to explain the membrane selectivity. In all samples the proton conductivity was less than that of Nafion117 and approached the latter linearly. However, relative methanol permeability showed drastic decreases above 50 °C. As the morphology approached a

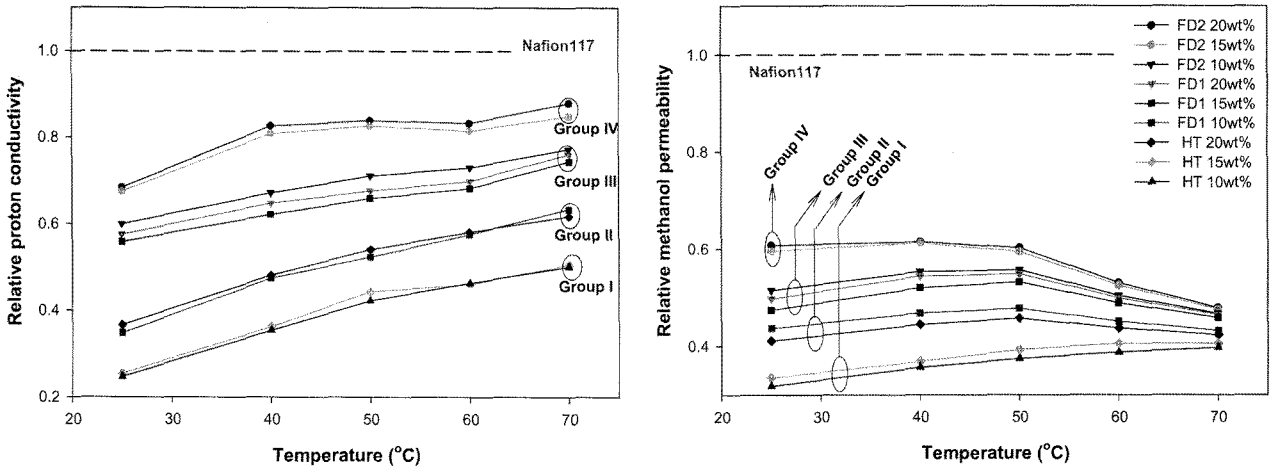

Figure 7. Relative transport properties.

co-continuous state the relative methanol permeability was further reduced.

Conclusions

Transport properties of blend membranes with various morphologies induced by different drying conditions were measured and analyzed on the basis of the absorbed water molecules. It was elucidated that both proton conductivity and methanol permeability could be correlated with the number of free water molecules. Group I, with a two layered structure, in spite of the sPAES-60 dominant bottom layer its RH-2000 rich upper layer blocked proton transport and methanol movement through the membrane. Because large hydrophilic domains in Group II were isolated from each other, the Group II membranes showed the lowest water uptake but their transport properties were higher than those of Group I because of higher free water concentration. Group III, with a nodular structure, formed better hydrophilic channels in the hydrated state, and thus higher proton conductivity and methanol permeability were measured due to the possibility of water passage through neighboring hydrophilic domains. Finally, well developed, co-continuous morphology in Group IV could be obtained. sPAES-60 and RH-2000 were three-dimensionally connected and hydrophilic and hydrophobic channels were also connected. Although the methanol permeability increased, hydrophilic channels facilitated proton movement and a hydrophobic network also restricted the free flow of large sized methanol molecules through the membrane. Consequently, fuel leakage was effectively limited. When the highly sulfonated copolymer (sPAES-60), which displays the highest proton conductivity but the highest methanol permeability, formed a co-continuous morphology with the non-sulfonated hydrophobic polymer (RH-2000), selectivity was maximized, and even at high temperature excellent selectivity was maintained due to the restriction of the enlargement of the hydrophilic channels by the neighboring continuous hydrophobic phase. Thus, layered morphology is not desirable in this regard, because it blocks proton transport as well as methanol leakage. In order to enhance the blend effect, co-continuous morphology is deemed the best choice and considered to be a good alternative to the perfluorinated ionomer membrane, which is expensive and vulnerable to the fuel leakage in DMFC applications.

Acknowledgement. The authors acknowledge Solvay Korea CO., LTD for supplying RH-2000.

References

(1) B. H. Steele and A. Heinzel, *Nature*, **414**, 345 (2001).
(2) K. Kordesch and G. Simader, *Fuel cells and Their Applications*, VCH Publishers Inc., New York, 1996.
(3) X. Ren, T. E. Springer, T. A. Zawodzinski, and S. Gottesfeld, *J. Electrochem. Soc.*, **147**, 466 (2000).
(4) S. Hikita, K. Yamane, and Y. Nakajima, *JSAE Rev.*, **22**, 151 (2001).
(5) J. Choi, I. T. Kim, S. C. Kim, and Y. T. Hong, *Macromol. Res.*, **13**, 514 (2005).
(6) J. C. Woong, S. Venkataramani, and S. C. Kim, *Polym. Int.*, **55**, 491 (2006).
(7) S. Swier, M. T. Shaw, and R. A. Weiss, *J. Membr. Sci.*, **270**, 22 (2006).
(8) K. D. Kreuer, *J. Membr. Sci.*, **185**, 29 (2001).
(9) J. T. Wang, J. S.Wainright, R. F. Savinell, and M. Litt, *J. Appl. Electrochem.*, **26**, 751 (1996).
(10) Y. Fu, A. Manthiram, and M. D. Guiver, *Electrochem. Comm.*, **8**, 1386 (2006).
(11) D. H. Kim, J. Choi, Y. T. Hong, and S. C. Kim, *J. Membr. Sci.*, **299**, 19 (2007).
(12) J. Won, J. Y. Yoo, M. -S. Kang, and Y. S. Kang, *Macromol. Res.*, **14**, 449 (2006).
(13) H. D. Cho, J. Won, H. Y. Ha, and Y. S. Kang, *Macromol. Res.*, **14**, 214 (2006).

(14) J. Li, C. H. Lee, H. B. Park, and Y. M. Lee, *Macromol. Res.*, **14**, 438 (2006).
(15) G. Y. Moon and J. W. Rhim, *Macromol. Res.*, **15**, 379 (2007).
(16) D. Seeliger, C. Hartnig, and E. Spohr, *Electrochim. Acta*, **50**, 4234 (2005).
(17) C. Manca, C. Tanner, and S. Leutwyler, *Int. Rev. Phys. Chem.*, **24**, 457 (2005).
(18) W. Xu and C. A. Angell, *Science*, **302**, 422 (2003).
(19) S. L. Chen, A. B. Bocarsly, and J. Benziger, *J. Power Sources*, **152**, 27 (2005).
(20) Y. S. Kim, L. Dong, M. A. Hickner, T. E. Glass, V. Webb, and J. E. McGrath, *Macromolecules*, **36**, 6281 (2003).
(21) B. S. Pivovar, Y. Wang, and E. L. Cussler, *J. Membr. Sci.*, **154**, 155 (1999).
(22) W. L. Harrison, M. A. Hickner, Y. S. Kim, and J. E. McGrath, *Fuel Cells*, **2**, 201 (2005).
(23) R. Y. Huang, P. Shao, X. Feng, and C. M. Burns, *J. Membr. Sci.*, **192**, 115 (2001).
(24) A. Siu, B. Pivovar, J. Horsfall, K. V. Lovell, and S. Holdcroft, *J. Polym. Sci. B*, **44**, 2240 (2006).
(25) A. Geoffrey, *Electrochemical Engineering Principles*, Prentice Hall, New Jersey, 1990.
(26) M. Saito, N. Arimura, K. Hayamizu, and T. Okada, *J. Phys. Chem. B*, **108**, 16064 (2004).